 doi:10.20944/preprints202107.0396.v1

Article

High-resolution Bistatic Wind Lidar

Paul Wilhelm *, Michael Eggert, Julia Hornig and Stefan Oertel

Physikalisch-Technische Bundesanstalt, Department 1.4 Gas Flow, Bundesallee 100, 38116 Braunschweig, Germany

* Correspondence: paul.wilhelm@ptb.de

Abstract: The high-resolution bistatic lidar developed at the Physikalisch-Technische Bundesanstalt (PTB) aims to overcome the limitations of conventional monostatic lidar technology which is widely used for wind velocity measurements in wind energy and meteorology applications. Due to the large measurement volume of a combined optical transmitter and receiver tilting in multiple directions, monostatic lidar generally has poor spatial and temporal resolution. It also exhibits large measurement uncertainty when operated in inhomogeneous flow, for instance, over complex terrain. In contrast, PTB's bistatic lidar uses three dedicated receivers arranged around a central transmitter, resulting in an exceptionally small measurement volume. The coherent detection and modulation schemes used allow the detection of backscattered, Doppler shifted light down to the scale of single aerosols, realising the simultaneous measurement of all three wind velocity components. This paper outlines design details and the theory of operation of PTB's bistatic lidar and provides an overview of selected comparative measurements. The results of these measurements have shown that the measurement uncertainty of PTB's bistatic lidar is well within the measurement uncertainty of traditional cup anemometers, while being fully independent of its site and traceable to the SI units. This allows its use as a transfer standard for the calibration of other remote sensing devices. Overall, PTB's bistatic lidar shows great potential to universally improve the capability and accuracy of wind velocity measurements, such as for the investigation of highly dynamic flow processes upstream and in the wake of wind turbines.

Keywords: wind lidar; Doppler lidar; bistatic; metrology; traceability; wind energy; meteorology

1. Introduction

Accurate wind velocity measurements are an essential prerequisite for many applications in the field of wind energy and meteorology, like wind potential analysis [1], power curve evaluations of wind turbines [2], and atmospheric turbulence analysis [3]. For example, low measurement uncertainties are especially desired for reliable resource assessments of projected wind farms because the wind turbine power output scales with the third power to the wind velocity [4]. Mandatorily, wind met masts with cup and sonic anemometers are used in these applications [5]. But they have the disadvantage of being inherently invasive and are thus prone to causing flow distortion effects [6]. Furthermore, taller masts covering hub heights of modern wind turbines are becoming economically less viable. Accordingly, ground-based wind lidar technology has become an alternative to wind met masts in the past few years, providing distortion-free remote measurement of true wind velocity [7,8].

Conventional *monostatic* wind lidar systems measure the wind velocity component in the direction of a common transmitting and receiving beam, utilising the Doppler shift of scattered light from aerosols passing the transmitting laser beam [9]. Monostatic lidar systems provide reliable results when operated over flat terrain and in undisturbed, that is, homogeneous flow [10]; however, these systems are not well suited for measurements over complex terrain. This is because the monostatic measurement principle can lead to measurement uncertainties in the order of 10 % when operated in inhomogeneous flow [11,12]. Figure 1 illustrates this problem of the monostatic measurement principle resulting from calculating the horizontal velocity based on the difference of varying radial wind velocities measured at different locations and times within a single measurement cycle. The measurement beam within the measurement cycle is tilted in different directions around

Preprints (www.preprints.org) | NOT PEER-REVIEWED | Posted: 19 July 2021 doi:10.20944/preprints202107.0396.v1

a circle with a height-dependant diameter of up to 100 m. Due to this dependence of the measurement uncertainty on the flow conditions at the measurement site, monostatic lidar systems are generally not traceable to SI units. They are thus not permitted to be used as transfer standards for the calibration of other remote sensing devices [13].

To overcome the aforementioned limitations and provide accurate and traceable measurements over any terrain, a *bistatic* wind lidar system has been developed at PTB. Figure 2 highlights the difference in operation of both lidar technologies. The conventional monostatic lidar (**a**) uses a rotating prism above a single combined transmitter and receiver unit scanning over a conical contour at different locations and times, with the beam's measurement volume extending up to 30 m in length [14]. In contrast, the bistatic PTB lidar (**b**) uses three dedicated receivers arranged at a radius of 1 m around a central transmitter, with all units being focused into a spatially highly resolved, ellipsoid-shaped measurement volume of a diameter $d = 300\ \text{m} \ldots 14\ \text{mm}$ and a length $l = 2\ \text{mm} \ldots 4\ \text{m}$ at heights ranging from 5 m to 200 m, respectively. This facilitates the simultaneous measurement of the three-dimensional wind velocity with exceptionally high spatial resolution, down to the scale of single aerosols. In consequence, the measurement uncertainty is largely independent of flow conditions at the measurement site. PTB's high-resolution bistatic lidar facilitates non-invasive wind velocity measurements at a sampling rate of up to 10 Hz (depending on the weather conditions at the measurement height) and is fully traceable to the SI units based upon the set-up's geometry, laser wavelength, and the digital time base used for frequency measurements.

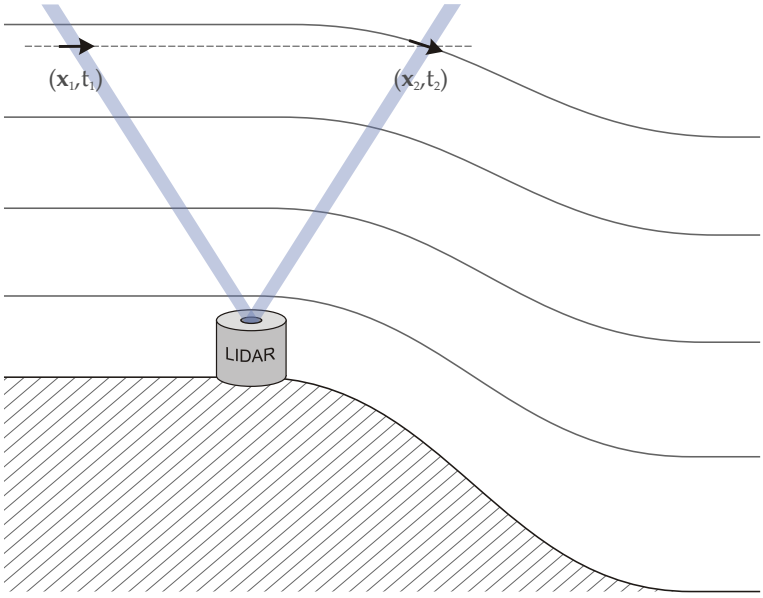

Figure 1. A monostatic lidar generally introduces a large measurement uncertainty when operating over complex terrain. This is the result of calculating the horizontal velocity based on the difference of varying radial wind velocities measured at different locations and times within a single measurement cycle in which the measurement beam is tilted in different directions.

Preprints (www.preprints.org) | NOT PEER-REVIEWED | Posted: 19 July 2021 doi:10.20944/preprints202107.0396.v1

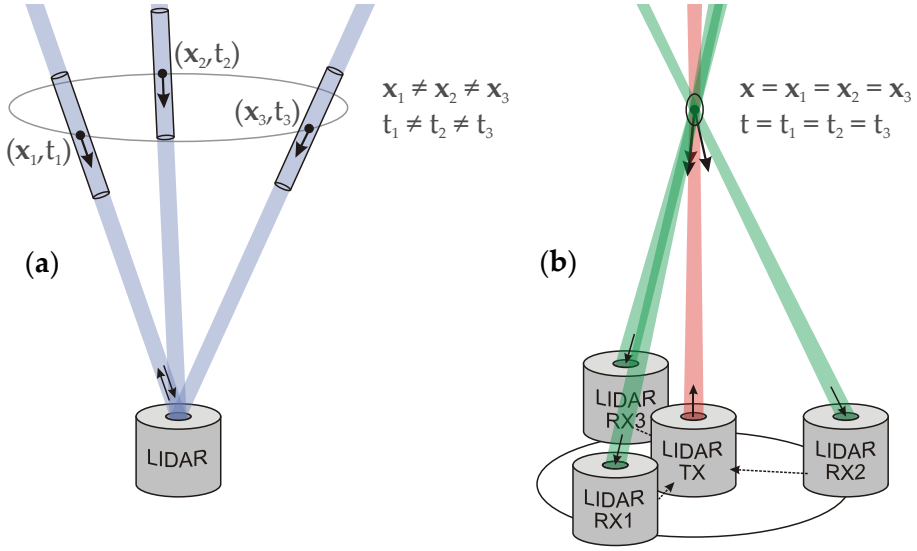

Figure 2. (**a**) A conventional monostatic lidar uses a single combined transmitter and receiver, resulting in a large measurement volume which needs to be multiplexed spatially and temporally by sequentially tilting the beam and sampling the wind speed. (**b**) The PTB bistatic lidar uses three separate receivers (*RX1*, *RX2*, *RX3*) around a central transmitter (*TX*), facilitating the simultaneous measurement of the three wind velocity components with high spatial and temporal resolution.

2. System Description

The PTB high-resolution bistatic lidar is mounted on a custom-designed trailer, providing increased mobility and suitability for long-term outdoor use. The hinged cover is closed during field operation but may be opened during development and servicing, as shown in figure 3. The sensitive optical set-up and the signal processing unit are located under the cover. To prevent vibrations during transport and operation, the optical set-up is mechanically decoupled from the trailer using air suspension. Further, to prevent the mechanical expansion and torsion of the optical carrier aluminium profile, the entire set-up is climatised to about 20 C using a 2 kW water-cooling unit. The transmitting laser amplifier is encased separately and water-cooled to reduce the excessive heating of the remaining set-up. Additional fans ensure sufficient air convection, and a dehumidifier prevents condensation forming on the optical windows inside the cover. [15]

The optical receivers are located at a radius of 1 m around the central transmitter in order to provide both sufficient backscattered light intensity (quasi-backwards, i.e. in a quasi-vertical direction) and sufficient resolution for determining the horizontal wind velocity component. Each receiver includes a servo-driven focus lens and a tilting mirror, as shown in figure 4. The tilting mirror is driven by a servo-piezo ensemble in order to provide sufficient resolution for the accurate positioning of the Gaussian beams at measurement heights of up to 250 m. As the transmitter does not need to be tilted, it only consists of a focus lens and a fixed mirror. Optically adjusting and focusing all the receivers and the transmitter into the small measurement volume is achieved by means of a specially developed scanning algorithm, successively approximating motor positions based on the received light intensity and measurement height.

The PTB high-resolution bistatic lidar uses coherent detection, processing the interference of the transmitted and backscattered light of aerosols carried along the flow [17]. While bistatic lidar technology generally poses the problem of low backscattered signal intensity, the received Doppler spectrum is concentrated into a significantly narrower bandwidth compared to that of conventional monostatic lidar. This is due to the more uniform motion of aerosols within the small measurement volume, allowing the detection of Doppler peaks with improved signal-to-noise ratio (SNR) [18]. At the receiver, the backscattered light of multiple aerosols with slightly different Doppler frequencies is detected [19]. Correlation techniques are used during signal processing, ensuring that only Doppler frequencies

 doi:10.20944/preprints202107.0396.v1

emitted by the same aerosol are evaluated [16]. The measurement height is first roughly determined by the theoretical height which is set using the optomechanical actuators, and it is finely determined by means of the difference in coherent phases of both Doppler shifted modulation peaks; due to the used modulation scheme the phases are periodic over the beam's length.

While the vertical wind velocity component directly generates an absolute Doppler shift to the backscattered light, the horizontal wind velocity component must be computed by means of correlated frequency offsets between all three receiving channels. Overall, due to the sharp angle between the transmitter beam and the receiver beam, detecting the vertical wind velocity component is orders of magnitude more sensitive than that of the horizontal wind velocity component [16]. With an average beam diameter of 10 mm between heights of 100 m to 200 m, the average transit time of a particle passing the measurement volume at a speed of 10 $\mathrm{m} \cdot \mathrm{s}^{-1}$ amounts to 1 ms. Both the reference laser's maximum bandwidth and the frequency resolution of the signal processing were chosen accordingly.

The optical set-up is constructed using single mode fibre optics internally, as shown in figure 5. A narrow-bandwidth (< 1 kHz) laser reference of a wavelength of 1550 nm is modulated using an acousto-optic modulator (AOM), amplified (up to 30 W CW) using an erbium-doped fibre amplifier (EDFA), and coupled into the transmitter beam optics. The received light is fed into fibre couplers, where it is coherently mixed (heterodyned) with the light of the reference laser; the resulting beat frequencies are the Doppler frequencies, converted down into a lower frequency range. Each optical mixing product is fed into a balanced photodetector (PD), where it is converted to an electrical signal that is ready to be processed.

The signal processing is performed in two steps: an FPGA pre-processes the signals at a high data rate, and a CPU post-processes these signals at a lower data rate. Both units are contained inside a common MicroTCA system carrier, transferring data via a high-speed backplane protocol. The FPGA has four analogue-digital converters (ADC) and four digital-analogue converters (DAC) associated with it, all interfaced using a fixed-latency protocol to ensure deterministic phase relationships within the coherent signal chain. The AOM modulation signal is provided using one of the available DACs; two spectral peaks at 75 MHz $\pm$ 12.5 MHz are added to the transmitted light intensity. These are necessary for determining the Doppler polarity, signal phase and, accordingly, the measurement height by means of spectral signal processing. Three of the ADCs are used for digitising the received signals, as shown in figure 6. The electrical signals from each balanced photodetector are subtracted and digitised using one dedicated ADC sampling at 300 MHz. Using the FPGA, the signal is mixed with a complex valued 75 MHz reference signal. The signal is then low-pass filtered and subsampled at a rate of 50 MHz. Finally, the signal is transmitted to the CPU, where it is transformed into the spectral domain using a fast Fourier transform (FFT) with a block length of 32768 samples, taking about 1 ms to complete. Further signal processing, such as filtering and correlating, typically increases the total computing time per sampling block to about 7 ms (which is only about 10 % of the theoretically achievable real-time performance).

Preprints (www.preprints.org) | NOT PEER-REVIEWED | Posted: 19 July 2021 doi:10.20944/preprints202107.0396.v1

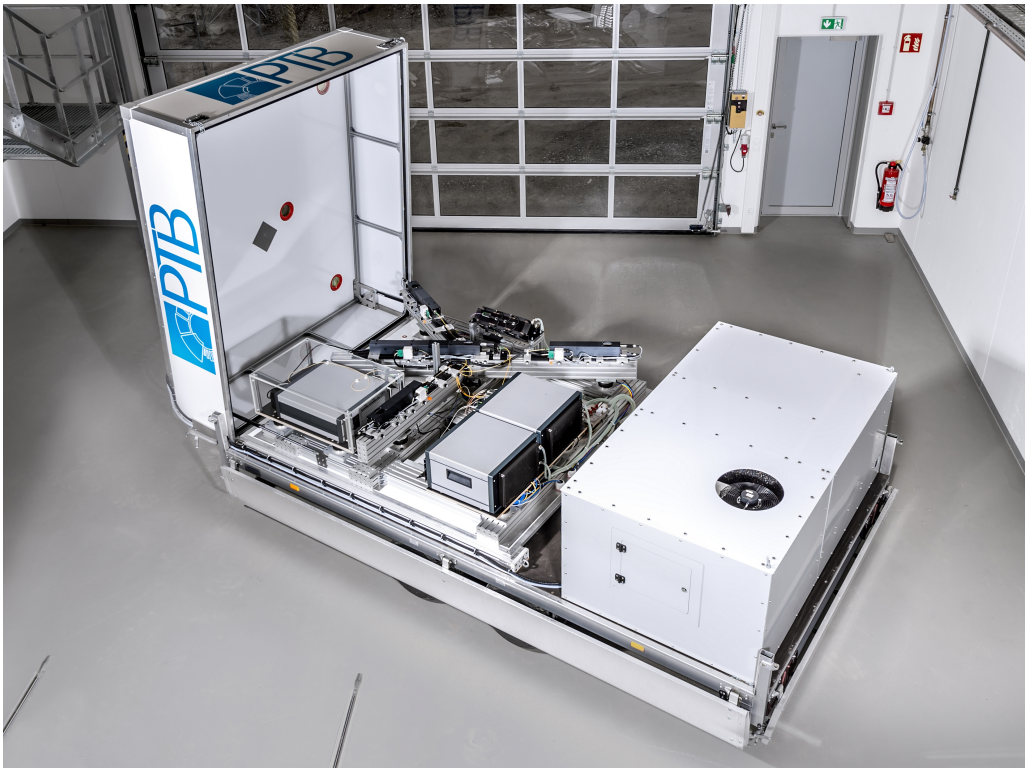

Figure 3. The PTB high-resolution bistatic lidar is mounted on a custom-designed trailer with a hinged cover (opened here), under which the optical set-up and signal processing unit are located. The water-cooling unit used for climatising this set-up is located within the box on the right-hand side.

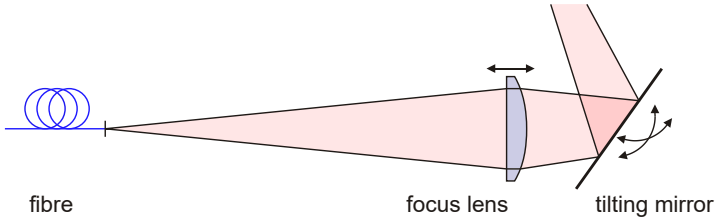

Figure 4. Principle of the optomechanical set-up: Each receiver consists of a servo-driven focus lens and a tilting mirror which is driven by a servo-piezo ensemble in order to provide sufficient resolution for accurate positioning at measurement heights up to 250 m. As the transmitter does not need to be tilted, it only consists of a focus lens and a fixed mirror.

Preprints (www.preprints.org) | NOT PEER-REVIEWED | Posted: 19 July 2021 doi:10.20944/preprints202107.0396.v1

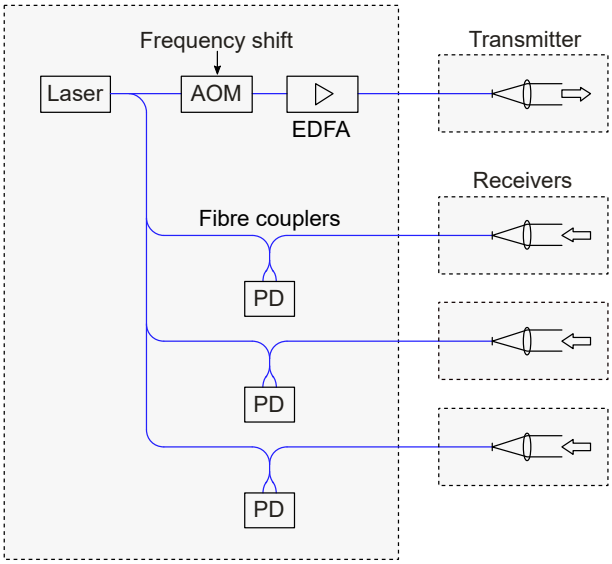

Figure 5. The optical set-up is constructed using fibre optics. A narrow-bandwidth laser reference is modulated, amplified, and fed into the transmitter beam optics. The light scattered back into the receiving beam optics is fed into fibre couplers, where it is coherently mixed with the reference laser's light. Each optical mixing product is fed into a balanced photodetector, where it is converted to an electrical signal.

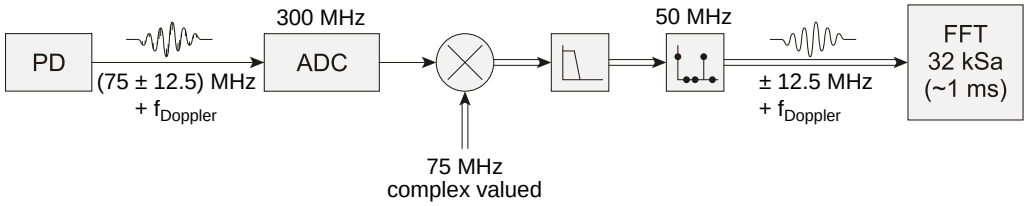

Figure 6. The electrical signals from each balanced photodetector are digitised using one dedicated ADC sampling at 300 MHz. The signal is then mixed with a complex valued 75 MHz reference signal, low-pass filtered and subsampled at a rate of 50 MHz. Finally, the signal is transformed into the spectral domain using an FFT with a block length of 32768 samples.

3. Validation and Characterisation

Since the development of PTB's high-resolution bistatic lidar started in 2010, several comparative measurements have been conducted in order to characterise this remote sensing device over a range of different operating conditions. Some of these measurements are described in the following sections.

3.1. PTB bistatic lidar / ultrasonic anemometer (Vaisala WMT700)

In 2014, the first comparative measurements between the PTB bistatic lidar and a Vaisala WMT700 ultrasonic anemometer mounted at a height of 10 m were conducted. Being representative of complex terrain, a common measurement site amidst several buildings at PTB was chosen. The measurements showed a very good agreement between the PTB bistatic lidar and the ultrasonic anemometer for both wind velocity magnitude and direction [20].

3.2. PTB bistatic lidar / monostatic lidar (WindCube)

In 2015, two comparative measurements between the PTB bistatic lidar and a monostatic lidar (WindCube) were conducted over flat terrain at PTB's antenna testing ground, and over complex terrain amidst several buildings at PTB. At each location, both devices were positioned at a distance of 10 m from each other and set to a measurement height of 100 m. Over flat terrain, both devices showed a good agreement with deviations below 1 %

 doi:10.20944/preprints202107.0396.v1

over a one-hour period of low atmospheric turbulence. However, over complex terrain, both devices showed significant deviations in the order of 15 %, as it is to be expected for measurements at different locations in turbulent flow and compared against conventional monostatic lidar technology [15].

3.3. PTB bistatic lidar / cup anemometers (135 m wind met mast) / monostatic lidar (WindCube)

In 2015 and 2016, two comparative measurements between the PTB bistatic lidar and a 135 m met mast equipped with several cup anemometers were conducted at the Deutsche WindGuard testing ground in Aurich, Germany. In 2015, a cup anemometer mounted on a boom at a height of 100 m was used for reference, and the PTB bistatic lidar was positioned nearby at a distance of about 1 m. In this situation, both devices were exposed to the *disturbed wake flow* of a nearby wind turbine. In 2016, the cup anemometer at the top of the met mast (135 m) was used for reference and the PTB bistatic lidar was positioned next to the met mast at a distance of about 3 m. For this second campaign, monostatic lidar (WindCube) data were also available and was incorporated into the comparative measurements. Wind velocity data were evaluated according to IEC 61400-12-1 [5], sorting horizontal wind speeds into discrete bins with a resolution of 0.5 $\mathrm{m \cdot s^{-1}}$.

Figure 7 shows the deviation between the PTB bistatic lidar and the boom-mounted anemometer in *disturbed flow* and for 1-second averaging intervals. Here, the PTB bistatic lidar shows deviations below 1 % over a large range of wind speeds from 6 $\mathrm{m \cdot s^{-1}}$ to 12 $\mathrm{m \cdot s^{-1}}$ when averaged over 1-second intervals. Figure 8 and figure 9 show the deviations between the PTB bistatic lidar and the top anemometer and between the monostatic lidar (WindCube) and the top anemometer in *undisturbed flow* for 10-minute and 1-minute averaging intervals, respectively. In *undisturbed flow*, for 10-minute averaging intervals and within bins in which at least 10 wind speeds were sampled, the PTB bistatic lidar's deviation with respect to the top anemometer reference amounts to less than 0.5 % (cf. figure 8), which is well within the cup anemometer's measurement uncertainty (roughly between ± 1 % at 4 $\mathrm{m \cdot s^{-1}}$ and ± 0.7 % at 13 $\mathrm{m \cdot s^{-1}}$). Under the same conditions, the monostatic lidar shows deviations up to -1.5 % (cf. figure 8). In *undisturbed flow* and for 1-second averaging intervals, the monostatic lidar shows large deviations (cf. figure 9). This is because it resorts to interpolation for intervals shorter than its native sampling interval, which comprises multiple seconds for a single scan. Contrastingly, under the *same conditions*, the PTB bistatic lidar's deviation only increases significantly beyond 1 % at very low or very high wind speeds. Extensive investigations and mathematical simulations showed that this is due to the different dynamic responses of the used sensing devices employed, and also due to the limited correlation of wind velocities sampled at slightly different locations [21].

Overall, owing to its high spatial and temporal resolution, the PTB bistatic lidar has been proven to achieve lower measurement uncertainty than conventional lidar systems, independent of the averaging time [21,22].

Preprints (www.preprints.org) | NOT PEER-REVIEWED | Posted: 19 July 2021 doi:10.20944/preprints202107.0396.v1

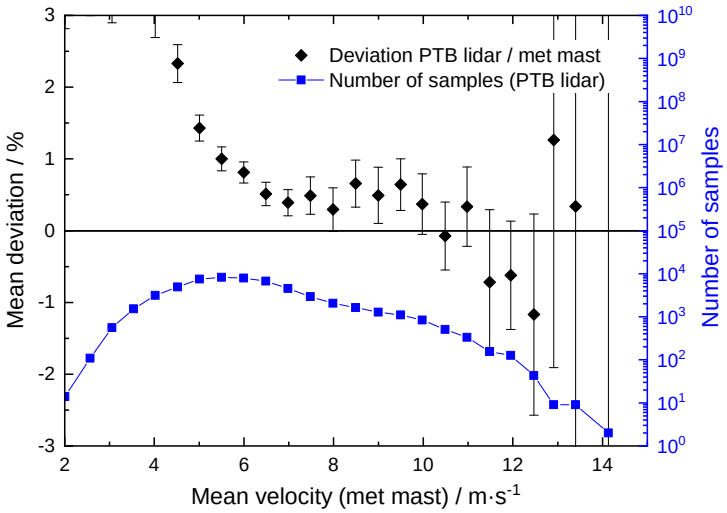

Figure 7. Results of the 2016 comparative measurement between the PTB bistatic lidar and a cup anemometer mounted on a met mast boom at a height of 100 m in *disturbed flow* at a measurement height of 100 m, evaluated according to IEC 61400-12-1 using 1-second intervals. The PTB bistatic lidar exhibits absolute deviations below 1 % over a large range of wind speeds from 6 $\mathrm{m \cdot s^{-1}}$ to 12 $\mathrm{m \cdot s^{-1}}$. The PTB bistatic lidar's deviation only increases significantly beyond 1 % at very low or very high wind speeds. Extensive investigations and mathematical simulations showed that this is due to the different dynamic responses of the used sensing devices employed, and also due to the limited correlation of wind velocities sampled at slightly different locations.

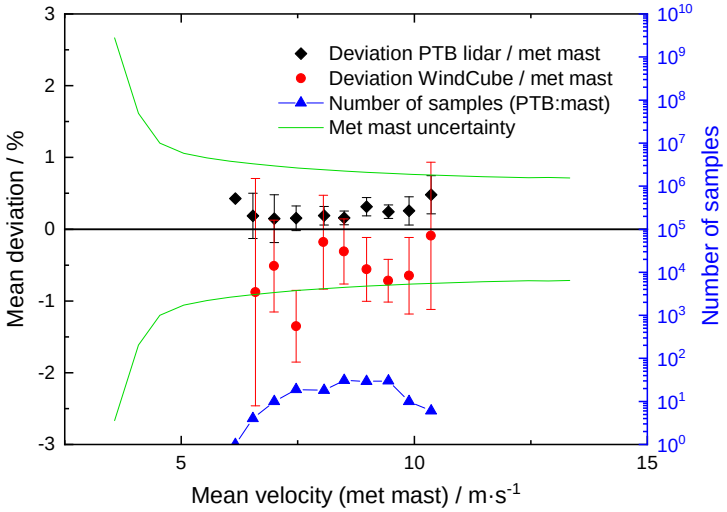

Figure 8. Results of the 2016 comparative measurement between the PTB bistatic lidar and the top anemometer and between the monostatic lidar (WindCube) and the top anemometer in *undisturbed flow* at a measurement height of 135 m, evaluated according to IEC 61400-12-1 using 10-minute intervals. For bins in which at least 10 values were obtained, the PTB bistatic lidar's deviation is less than 0.5 %, which is well within the cup anemometer's measurement uncertainty (roughly between ± 1 % at 4 $\mathrm{m \cdot s^{-1}}$ and ± 0.7 % at 13 $\mathrm{m \cdot s^{-1}}$). Under the same conditions, the monostatic lidar shows deviations up to -1.5 %.

Preprints (www.preprints.org) | NOT PEER-REVIEWED | Posted: 19 July 2021 doi:10.20944/preprints202107.0396.v1

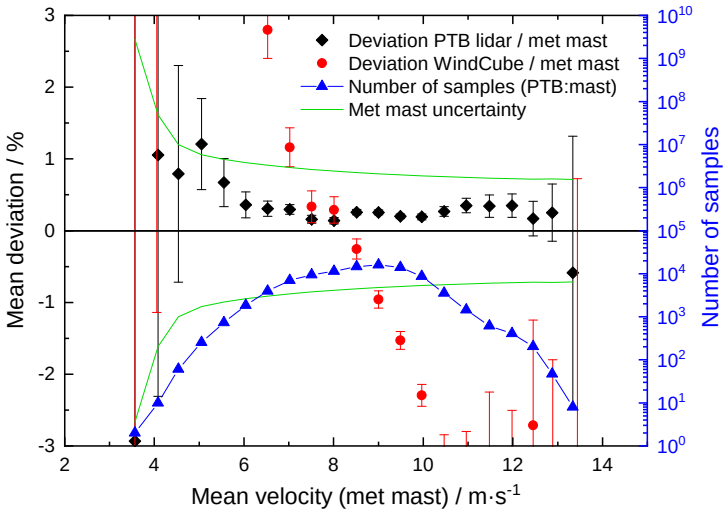

Figure 9. Results of the 2016 comparative measurement between the PTB bistatic lidar and the top anemometer and between the monostatic lidar (WindCube) and the top anemometer in *undisturbed flow* at a measurement height of 135 m, evaluated according to IEC 61400-12-1 using 1-second intervals. The monostatic lidar shows large deviations, while the PTB bistatic lidar's deviation only increases significantly beyond 1 % at very low or very high wind speeds.

3.4. PTB bistatic lidar / LDV in wind tunnel

In 2018, the PTB bistatic lidar was characterised in a wind tunnel at PTB's Competence Center for Wind Energy (CCW). It was shown that the wind tunnel provides a well-defined, homogeneous velocity field suitable for calibrations [23]. Being specifically constructed for the validation of the PTB bistatic lidar, the wind tunnel is mounted on a platform at a height of 8 m, allowing the PTB bistatic lidar trailer to be positioned right below it for sensing its velocity field. An LDV (laser Doppler velocimeter) was used as a referenced standard, as these devices have measurement uncertainties below 0.2 % [13], which is lower than the measurement uncertainties achievable with cup anemometers (roughly between ± 0.7 % and ± 1 %). Figure 10 shows the deviation of the PTB bistatic lidar to the LDV. These first validation measurements of wind speeds ranging from 4 $\mathrm{m \cdot s^{-1}}$ to 16 $\mathrm{m \cdot s^{-1}}$ showed an average deviation of 0.37 % between the LDV and the PTB high-resolution bistatic lidar [24,25].

Preprints (www.preprints.org) | NOT PEER-REVIEWED | Posted: 19 July 2021 doi:10.20944/preprints202107.0396.v1

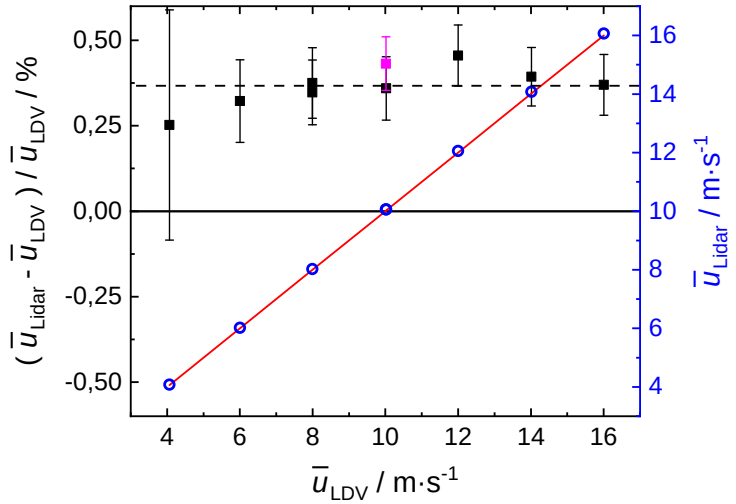

Figure 10. Results of the 2018 comparative measurement between the PTB bistatic lidar and an LDV in a wind tunnel at PTB's Competence Center for Wind Energy, showing an average deviation of 0.37 % between both devices. In order to verify that the PTB bistatic lidar is free of any angular dependence, an additional sample was recorded at 10 m · s^{-1} (shown in pink) after the PTB bistatic lidar trailer was rotated 90.

3.5. PTB bistatic lidar / sonic anemometer (CSAT3B) in turbulent flow

In 2019, a comparative measurement between the PTB bistatic lidar and a CSAT3B ultrasonic anemometer mounted on top of a 30 m mast was conducted over flat terrain at the site of the Johann Heinrich von Thünen Institut (the German Federal Research Institute for Rural Areas, Forestry and Fisheries) in Braunschweig, Germany. At this height, the PTB bistatic lidar's measurement volume (diameter $d = 2$ mm and length $l = 50$ mm) is comparable to that of the used sonic anemometer. The PTB bistatic lidar was positioned 9 m away from the mast, and both devices sampled wind velocity data at a rate of 10 Hz over a period of about two weeks.

Figure 11 shows the orthogonal linear regressions of the average horizontal wind velocity component $\overline{u}$, of the fluctuation of the vertical wind velocity component $\overline{w'w'}^{1/2}$, and of the shear stress velocity u_*. Table 1 shows the corresponding statistical parameters. Both devices showed a very good agreement, especially for the fluctuation of the vertical wind velocity component which shows a mean deviation of only 0.017 m · s^{-1} at an intercept of -0.009 m · s^{-1} and a slope of 0.989. Also, there is a good agreement for the average horizontal wind velocity component $\overline{u}$ with an intercept of 0.044 m · s^{-1} and a slope of also 0.989. However, at a slope of 0.973, the shear stress velocity u_* exhibits a slightly larger deviation from unity. This is demonstrably due to the angular dependence inherent to ultrasonic anemometers.

The dynamics of fully developed turbulence in the inertial subrange (an intermediate range of scales within the underlying energy cascade) can be described by certain similarity laws [26]. Specifically, the ensemble cospectrum (spectrum of the cross-correlation of two orthogonal velocity components) follows a $-7/3$ power law [27]. Figure 12 shows the ensemble cospectra Co_{uw} between the wind velocity components u and w of the PTB bistatic lidar and the CSAT3B sonic anemometer. The PTB high-resolution bistatic lidar is in excellent agreement with the theoretical distribution, showing a drop-off in cospectral power density consistent with the theoretical $-7/3$ law. However, due to its angular dependence, at higher frequencies the CSAT3B sonic anemometer deviates significantly from the theoretical distribution.

Overall, although both the PTB bistatic lidar and the employed ultrasonic anemometer have proven to be well suited for measurements in turbulent flow, the PTB bistatic lidar is the more favourable option if high precision is desired. This is due to its distortion-free measurement capability which is free of any angular dependence [3,28].

Preprints (www.preprints.org) | NOT PEER-REVIEWED | Posted: 19 July 2021 doi:10.20944/preprints202107.0396.v1

Table 1. Statistical parameters of the 2019 comparative measurement between the PTB bistatic lidar and a CSAT3B ultrasonic anemometer mounted on top of a 30 m mast.

	$\overline{u}$	$\overline{w'w'}^{1/2}$	u_*
Bias ($m \cdot s^{-1}$)	0.003	-0.009	-0.009
Mean deviation, RMSE ($m \cdot s^{-1}$)	0.082	0.017	0.042
Regression: intercept ($m \cdot s^{-1}$)	0.044	-0.009	0.000
Regression: slope	0.989	0.989	0.973
Correlation coefficient	0.998	0.998	0.980

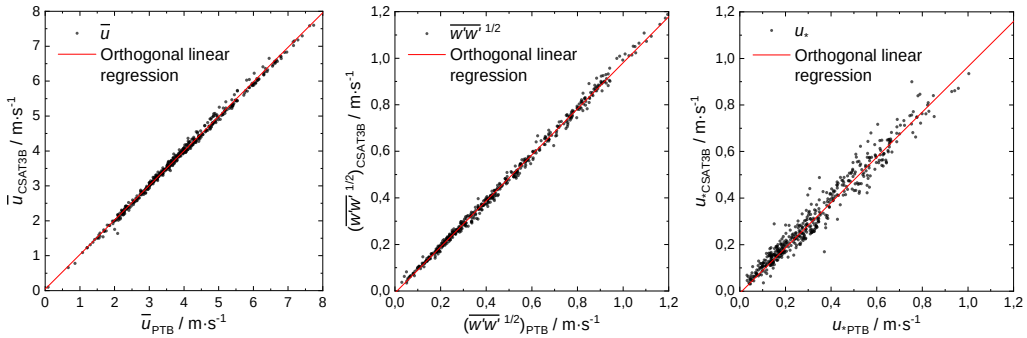

Figure 11. Results of the 2019 comparative measurement between the PTB bistatic lidar and a CSAT3B ultrasonic anemometer mounted on top of a 30 m mast in turbulent flow, showing orthogonal linear regressions of the average horizontal wind velocity component $\overline{u}$, of the fluctuation of the vertical wind velocity component $\overline{w'w'}^{1/2}$, and of the shear stress velocity u_*.

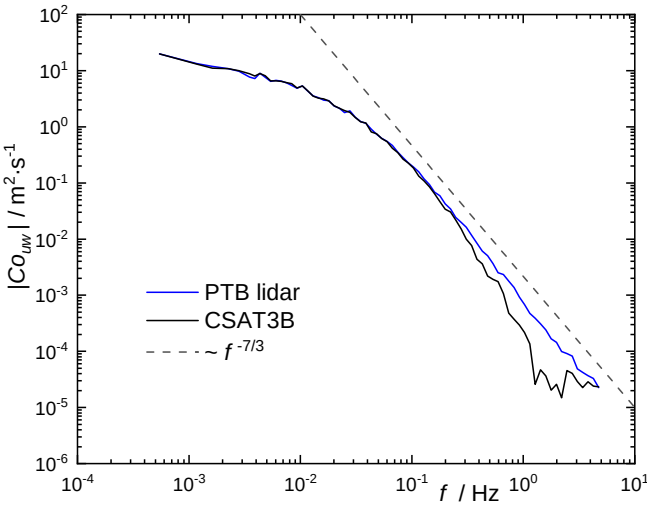

Figure 12. Results of the 2019 comparative measurement between the PTB bistatic lidar and a CSAT3B ultrasonic anemometer mounted on top of a 30 m mast in turbulent flow, showing the ensemble cospectra Co_{uw} between the wind velocity components u and w (absolute values) of the PTB bistatic lidar and the CSAT3B sonic anemometer. The dashed line indicates the theoretical $-7/3$ power law in the inertial subrange.

3.6. PTB bistatic lidar / cup anemometer (200 m wind met mast)

In 2020, a comparative measurement between the PTB bistatic lidar and a Thies Clima First Class Advanced cup anemometer mounted on top of a 200 m met mast was conducted near the summit of the Rödeser Berg near Kassel, Germany. Both the PTB bistatic lidar and the top cup anemometer were measuring at a height of 200 m for about three weeks.

Preprints (www.preprints.org) | NOT PEER-REVIEWED | Posted: 19 July 2021 doi:10.20944/preprints202107.0396.v1

Additionally, wind direction data were obtained from a Thies Clima First Class wind vane mounted on a boom of the wind met mast at a height of 187 m.

Figure 13 shows the overall measurement site which includes two wind turbines (a third wind turbine located south-east is not shown). The PTB bistatic lidar trailer was positioned next to the met mast at a distance of 4.6 m. All angles stated in this section are referenced to the 0 north direction and counting in a clockwise direction (meteorological wind direction). Multiple pairs of oppositely mounted booms are located at different heights on the wind met mast at 145 and 325 angles. The wind turbines are located at 146 and 307 angles.

Figure 14 shows the deviation of the PTB bistatic lidar to the top anemometer for *unfiltered* 10-minute averaged wind speeds larger than 4 $m \cdot s^{-1}$. However, these unfiltered samples are problematic in two ways. Firstly, large perturbation effects due to the wind met mast's booms are visible around 145 and 325 angles, and secondly, due to the PTB bistatic lidar's optical measurement principle, fog occasionally causes large, non-systematic deviations which are clearly visible between 90 and 270 angles. Thus, to enable a more reasonable comparison, the data were filtered around the boom angles, and periods of fog were filtered using an upper limit on the backscattered signal amplitude. Figure 15 shows the deviation between the PTB bistatic lidar and the top anemometer for *filtered* 10-minute averages, now indicating a good agreement between both instruments with absolute deviations below 2.5 %.

Figure 16 shows the deviation between the PTB bistatic lidar and the top anemometer for filtered wind speeds ranging from 4 $m \cdot s^{-1}$ to 19.5 $m \cdot s^{-1}$. Here, wind velocity data were evaluated according to IEC 61400-12-1 [5], sorting horizontal wind speeds into discrete bins with a resolution of 0.5 m $\cdot$ s^{-1}. Again, both the PTB bistatic lidar and the top anemometer show a good agreement with mean deviations below 0.5 % over a large range of wind speeds. Figure 17 shows the linear orthogonal regression of the wind directions measured by the PTB bistatic lidar and the wind vane mounted on the met mast. With an intercept of 3.736 and a slope of 0.996, both instruments are in excellent agreement regarding the measured wind direction.

Overall, the directional effects inherent to the wind met mast's structure and the PTB bistatic lidar's sensitivity to periods of fog necessitated additional filtering of the data obtained in this particular comparative measurement campaign. Nevertheless, both the PTB bistatic lidar and the wind met mast's top anemometer show a good agreement with mean deviations below 0.5 % over a large range of wind speeds. Furthermore, the wind directions as measured by the PTB bistatic lidar and the wind vane mounted on the met mast are in excellent agreement.

Preprints (www.preprints.org) | NOT PEER-REVIEWED | Posted: 19 July 2021 doi:10.20944/preprints202107.0396.v1

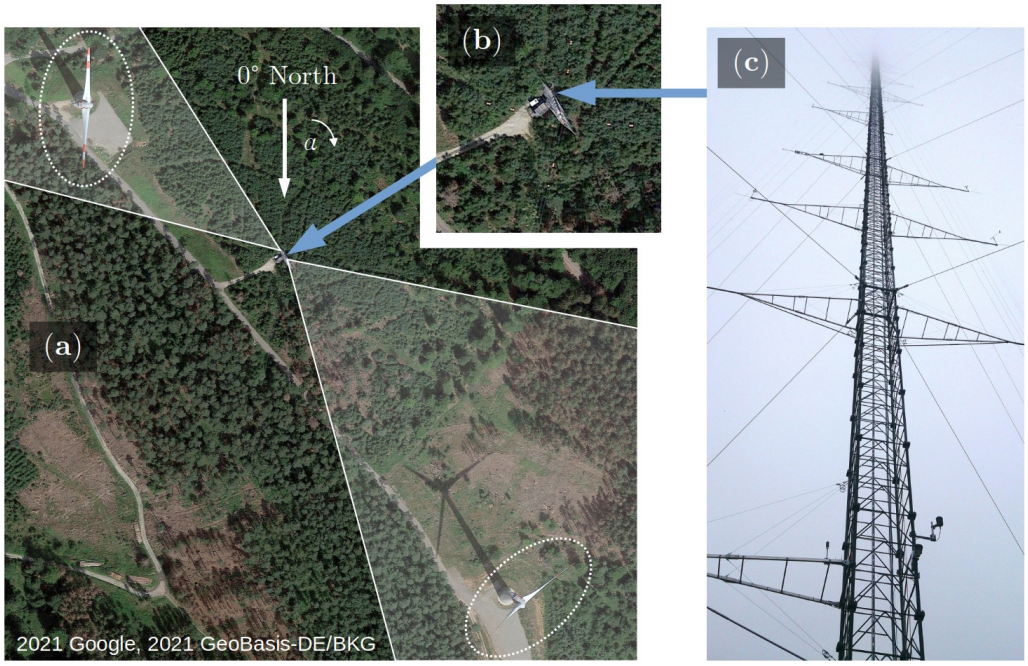

Figure 13. (**a**) Measurement site including two wind energy turbines located at 146 and 307 angles (a third wind turbine located south-east is not shown). Around the met mast, the areas corresponding to the wakes of the nearby wind turbines are highlighted between 100 to 165 and 285 to 330 angles. (**b**) Slightly larger view of the wind met mast and its orientation with respect to the measurement site. (**c**) Met mast with multiple booms mounted at different heights and at 145 and 307 angles.

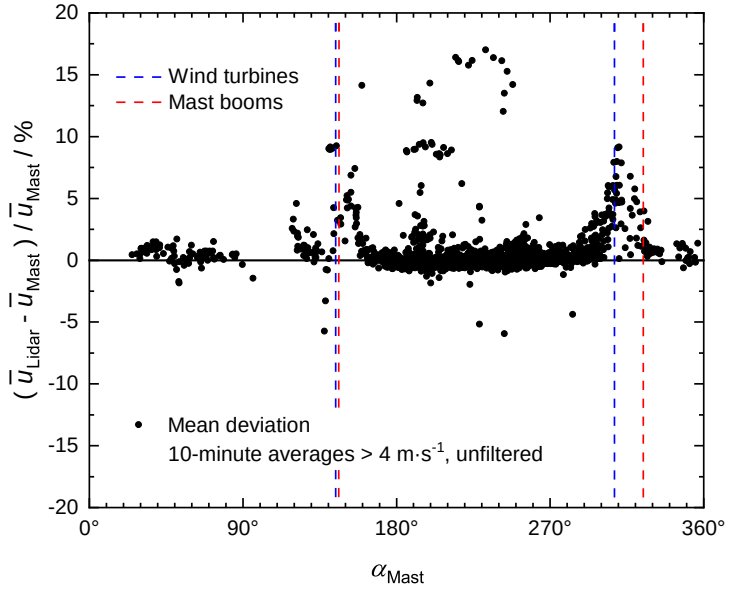

Figure 14. Results of the 2020 comparative measurement between the PTB bistatic lidar and a cup anemometer mounted on top of a 200 m met mast, showing the directional dependence of the mean deviation between the PTB bistatic lidar and the top anemometer for *unfiltered* 10-minute averages. Large perturbation effects due to the structure of the wind met mast and its booms are visible around angles 145 and 325. Additionally, fog occasionally causes very large, non-systematic deviations which are clearly visible between 90 and 270 angles.

Preprints (www.preprints.org) | NOT PEER-REVIEWED | Posted: 19 July 2021 doi:10.20944/preprints202107.0396.v1

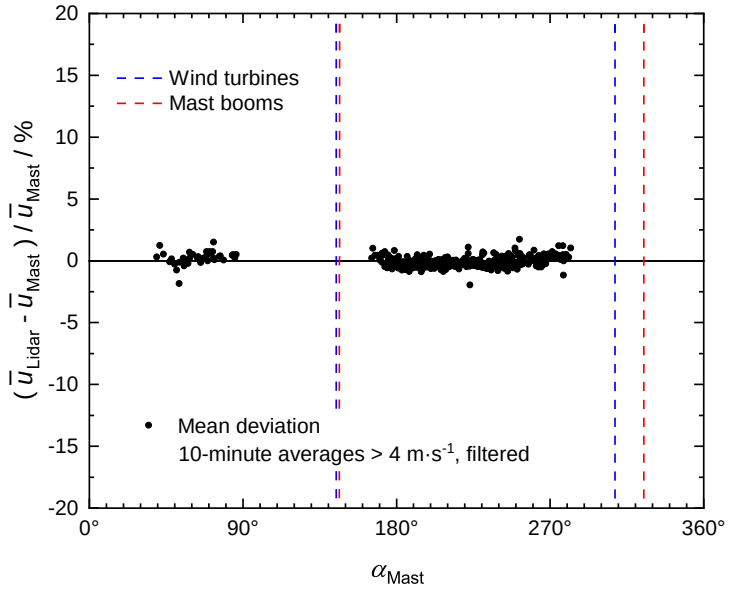

Figure 15. Results of the 2020 comparative measurement between the PTB bistatic lidar and a cup anemometer mounted on top of a 200 m met mast, showing the directional dependence of mean deviation between the PTB bistatic lidar and the top anemometer for *filtered* 10-minute averages. Perturbation effects due to the wind met mast booms have been reduced by directional filtering. Also, periods of fog were excluded from the data.

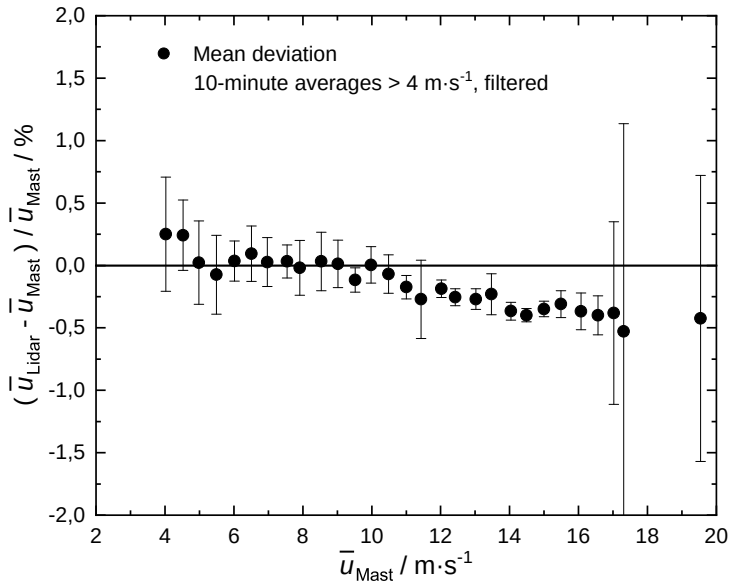

Figure 16. Results of the 2020 comparative measurement between the PTB bistatic lidar and a cup anemometer mounted on top of a 200 m met mast, evaluated according to IEC 61400-12-1 using filtered 10-minute averages. Both instruments show good agreement with mean deviations between $+0.25$ % and -0.5 % over a large range of wind speeds.

Preprints (www.preprints.org) | NOT PEER-REVIEWED | Posted: 19 July 2021 doi:10.20944/preprints202107.0396.v1

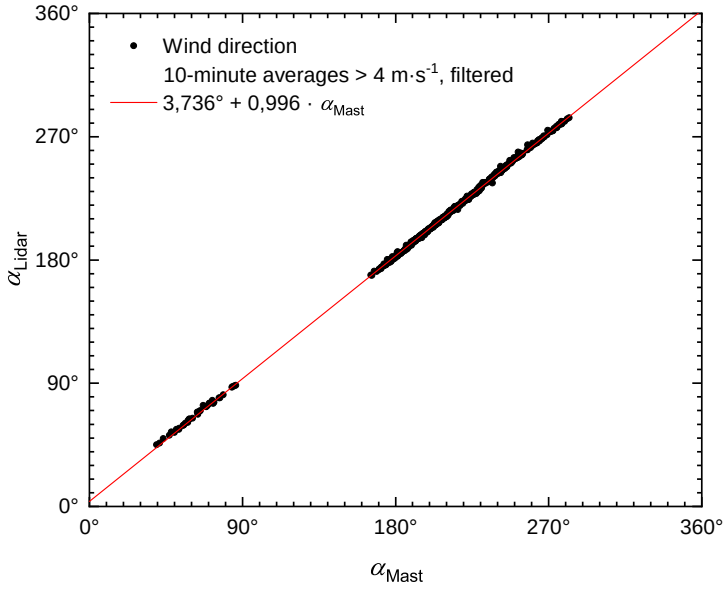

Figure 17. Results of the 2020 comparative measurement between the PTB bistatic lidar and a cup anemometer mounted on top of a 200 m met mast, showing the linear orthogonal regression of the filtered wind directions measured by the PTB bistatic lidar and the wind vane mounted on the met mast.

4. Conclusions and Outlook

This paper has outlined design details and the theory of operation of PTB's high-resolution bistatic lidar. It has also provided an overview of selected comparative measurements. The comparative measurements between the PTB bistatic lidar and the cup anemometers mounted on the met masts have shown that the measurement uncertainty of PTB's bistatic lidar is well within the measurement uncertainty of traditional cup anemometers (roughly between ± 1 % at 4 m $\cdot$ s^{-1} and ± 0.7 % at 13 m $\cdot$ s^{-1}) while being fully independent of its site. The comparative measurement between the PTB bistatic lidar and an industry-standard ultrasonic anemometer (CSAT3B) in turbulent flow has shown that the PTB bistatic lidar provides distortion-free measurement capability which is free of any angular dependence and in excellent agreement with the theoretical $-7/3$ power law in the inertial subrange.

To summarise, the high-resolution bistatic lidar developed at PTB has been proven to provide spatially and temporally highly resolved remote measurements of the wind velocity at heights ranging from 5 m to 200 m over any terrain. Furthermore, it provides measurement results with exceptionally low measurement uncertainty that are traceable to the SI units. Thus, it is planned to use the PTB high-resolution bistatic lidar as a transfer standard for other wind velocity remote sensing devices in the future. Overall, the PTB bistatic lidar shows great potential to universally enhance the capability and accuracy of measurements in applications, like wind potential analysis, the power curve evaluation of wind turbines and atmospheric turbulence analysis.

Nevertheless, there is still room for improvement. Adjusting the measurement height is currently slow, requiring multiple scans over an interval of several minutes. Therefore, the optomechanical section is being completely reworked. This is moreover being combined with an improved signal processing unit using the latest radio-frequency system-on-chip (RFSoC) technology. In the future, this will enable the fast and autonomous selection of measurement heights, allowing the PTB bistatic lidar to perform wind profile measurements. The improved signal processing will take the performance closer to real-time, increasing both the spectral resolution and the number of aerosols detectable per unit of time, which is also a requirement for fast beam alignment.

Several desirable functionalities and improvements are still missing from the PTB bistatic lidar at its current stage. Firstly, because of the PTB bistatic lidar's optical mea-

surement principle, its measurement capability is degraded during weather conditions, such as precipitation and fog. It is thus desirable to incorporate the automatic detection and mitigation of these conditions based upon the SNR and other spectral characteristics of the received Doppler spectra. Secondly, a thorough investigation of the measurement uncertainty as a function of the SNR and the characteristic distributions of correlated Doppler peaks for varying meteorological conditions is needed in order to improve upon the achieved measurement uncertainty by fine-tuning the digital signal processing chain. These are only some of the aspects that are to be addressed over the course of the coming years in order to provide a fully autonomous remote sensing device which is suitable for use as a transfer standard.

Author Contributions: Conceptualization, M. Eggert; methodology, M. Eggert; software, P. Wilhelm, M. Eggert; validation, M. Eggert; formal analysis, M. Eggert; investigation, M. Eggert, P. Wilhelm; data curation, M. Eggert, P. Wilhelm; writing—original draft preparation, P. Wilhelm; writing—review and editing, P. Wilhelm, M. Eggert, J. Hornig; visualization, M. Eggert, P. Wilhelm, S. Oertel; supervision, H. Többen; project administration, J. Hornig; funding acquisition, H. Többen, J. Hornig, P. Wilhelm. All authors have read and agreed to the published version of the manuscript.

Funding: This research was funded by the German Federal Ministry for Economic Affairs and Energy (BMWi), funding codes 0325416B (*WindLidarDSP*) and 0325945 (*PTB Wind*).

Data Availability Statement: The data presented in this study are available upon request from the corresponding author. The data are not publicly available due to third party agreements. Data were obtained from Deutsche WindGuard GmbH, the Karlsruhe Institute of Technology, the Carl von Ossietzky University Oldenburg and the Fraunhofer Institute for Energy Economics and Energy System Technology.

Acknowledgments: We thank Deutsche WindGuard GmbH (Varel, Germany), the Karlsruhe Institute of Technology (Garmisch-Partenkirchen, Germany), the Carl von Ossietzky University Oldenburg (Oldenburg, Germany) and the Fraunhofer Institute for Energy Economics and Energy System Technology (Kassel, Germany) for making the joint measurement campaigns possible.

Conflicts of Interest: The authors declare no conflict of interest. The funders had no role in the design of the study; in the collection, analyses, or interpretation of data; in the writing of the manuscript, or in the decision to publish the results.

Abbreviations

The following abbreviations are used in this manuscript:

ADC	Analogue-digital converter
AOM	Acousto-optic modulator
CCW	Competence Center for Wind Energy
DAC	Digital-analogue converter
EDFA	Erbium-doped fibre amplifier
FFT	Fast Fourier transform
FPGA	Field-programmable gate array
LDV	Laser Doppler velocimeter
Lidar	Light detection and ranging
SNR	Signal-to-noise ratio
PD	Photodetector
PTB	Physikalisch-Technische Bundesanstalt

References

1. MEASNET. Evaluation of Site-Specific Wind Conditions, Version 2, April 2016. Available online: https://www.measnet.com/wp-content/uploads/2016/05/Measnet_SiteAssessment_V2.0.pdf (accessed on 4 March 2021).
2. Scheurich, F.; Enevoldsen, P.B.; Paulsen, H.N.; Dickow, K.K.; Fiedel, M.; Loeven, A.; Antoniou, I. Improving the Accuracy of Wind Turbine Power Curve Validation by the Rotor Equivalent Wind Speed Concept. *J. Phys. Conf. Ser.* **2008**, *753*, 072029.

3. Mauder, M.; Eggert, M.; Gutsmuths, C.; Oertel, S.; Wilhelm, P.; Voelksch, I.; Wanner, L.; Tambke, J.; Bogoev, I. Comparison of turbulence measurements by a CSAT3B sonic anemometer and a high-resolution bistatic Doppler lidar. *Atmos. Meas. Tech.* **2020**, *13*, 969–983.
4. Kalmikov, A. Wind Power Fundamentals. Available online: http://web.mit.edu/wepa/WindPowerFundamentals.A.Kalmikov.2017.pdf (accessed on 4 March 2021).
5. IEC 61400-12-1 *Wind energy generation systems – Part 12-1: Power performance measurements of electricity producing wind turbines*, 2nd ed.; 2017.
6. Lindelöw, P.J.P.; Friis Pedersen, T.; Gottschall, J.; Vesth, A.; Wagner, R.; Schmidt Paulsen, U.; Courtney, M. Flow distortion on boom mounted cup anemometers. *Denmark. Forskningscenter Risoe. Risoe-R* **2010**, *1738(EN)*.
7. Albers, A.; Janssen, A.W.; Mander, J. How to gain acceptance for lidar measurements. Available online: https://www.windguard.de/veroeffentlichungen.html (accessed on 4 March 2021).
8. Slinger, C.; Harris, M. Introduction to continuous-wave Doppler lidar. Available online: http://breeze.colorado.edu/ftp/RSWE/Chris_Slinger.pdf (accessed on 4 March 2021).
9. Drain, L.E. *The Laser Doppler Technique*, 1st ed.; Publisher: John Wiley & Sons, New York, 1980.
10. Gottschall, J.; Courtney, M.S.; Wagner, R.; Jørgensen, H.E.; Antoniou, I. Lidar profilers in the context of wind energy – A verification procedure for traceable measurements. *Wind Energ.* **2012**, *15*, 147–159.
11. Bradley, S. Wind speed errors for LIDARs and SODARs in complex terrain. *IOP Conf. Ser.: Earth Environ. Sci.*, **2008**, *1*.
12. Bingöl, F.; Mann, J.; Foussekis, D. Conically scanning lidar error in complex terrain. *Meteorol. Z.*, **2009**, *18*, 189–195.
13. Müller, H.; Pape, N.; Eggert, M.; Westermann, D.; Albers, A. Bedeutung laseroptischer Verfahren für die Windgeschwindigkeitsmessung. *Experimentelle Strömungsmechanik*, **2010**, *18*.
14. Ando, T.; Kameyama, S.; Hirano, Y. All-fiber coherent Doppler LIDAR technologies at Mitsubishi Electric Corporation. *IOP Conf. Ser.: Earth Environ. Sci.*, **2008**, *1*.
15. Gutsmuths, C.; Eggert, M.; Müller, H.; Többen, H. Zeitaufgelöste, vektorielle Vergleichsmessungen zwischen dem Doppler-LIDAR-Transfernormal der PTB und konventionellen LIDAR-Systemen. *Experimentelle Strömungsmechanik*, **2015**, *23*.
16. Eggert, M.; Müller, H.; Többen, H. Doppler-Lidar-Transfernormal zur ortsaufgelösten, vektoriellen Windgeschwindigkeitsmessung. *Experimentelle Strömungsmechanik*, **2013**, *21*.
17. Harris, M.; Constant, G.; Ward, C. Continuous-wave bistatic laser Doppler wind sensor. *Appl. Opt.*, **2001**, *40*, 1501–1506.
18. Eggert, M.; Müller, H.; Többen, H. Doppler-Lidar-Transfernormals zur Windgeschwindigkeitsmessung: Aktueller Entwicklungsstand. *Experimentelle Strömungsmechanik*, **2012**, *20*.
19. Eggert, M.; Müller, H.; Többen, H. Konzeption eines Doppler-Lidar-Transfernormals zur Windgeschwindigkeitsmessung. *Experimentelle Strömungsmechanik*, **2011**, *19*.
20. Eggert, M.; Gutsmuths, C.; Müller, H.; Többen, H. Zeitaufgelöste, vektorielle Vergleichsmessungen zwischen dem Doppler-Lidar-Transfernormal der PTB und einem Referenz-Ultraschallanemometer. *Experimentelle Strömungsmechanik*, **2014**, *22*.
21. Eggert, M.; Gutsmuths, C.; Oertel, S.; Müller, H.; Többen, H. Untersuchungen zur Vergleichbarkeit von instantanen Strömungsgeschwindigkeitsmessungen des bistatischen Doppler-Lidars der PTB und trägheitsbehafteten Messungen eines Schalensternanemometers. *Experimentelle Strömungsmechanik*, **2017**, *25*.
22. Eggert, M.; Gutsmuths, C.; Müller, H.; Többen, H. Zeitaufgelöste, vektorielle Vergleichsmessungen zwischen dem Doppler-Lidar-Transfernormal der PTB und einem 135 m hohen Windmessmasten. *Experimentelle Strömungsmechanik*, **2016**, *24*.
23. Oertel, S.; Eggert, M.; Gutsmuths, C.; Wilhelm, P.; Müller, H.; Többen, H. Windkanalmesseinrichtung für die Validierung des bistatischen PTB-Wind-Lidars als Bezugsnormal. *Experimentelle Strömungsmechanik*, **2018**, *26*.
24. Oertel, S.; Eggert, M.; Gutsmuths, C.; Wilhelm, P.; Müller, H.; Többen, H. Bistatic wind lidar system for traceable wind vector measurements with high spatial and temporal resolution. *FLOMEKO*, **2019**, *18*.
25. Oertel, S.; Eggert, M.; Gutsmuths, C.; Wilhelm, P.; Müller, H.; Többen, H. Validation of three-component wind lidar sensor for traceable highly resolved wind vector measurements. *J. Sens. Sens. Syst.*, **2019**, *8*, 9–17.
26. Kolmogorov, A.N. The local structure of turbulence in incompressible viscous fluid for very large Reynolds numbers. *C. R. Acad. Sci. URSS*, **1941**, *30*, 301–305.
27. Kaimal, J.C.; Finnigan, J.J. *Atmospheric Boundary Layer Flows: Their Structure and Measurement.*; Publisher: Oxford University Press, New York, 1994.
28. Eggert, M.; Tambke, J.; Gutsmuths, C.; Oertel, S.; Wilhelm, P.; Müller, H.; Mauder, M. Vergleich des bistatischen Doppler-Lidars der PTB und eines Ultraschall-Anemometers zur Messung von Turbulenzspektren. *Experimentelle Strömungsmechanik*, **2019**, *27*.